Internal Constitution and Equation of State of Neutron-Star Crusts Within the Nuclear Energy Density Functional Theory

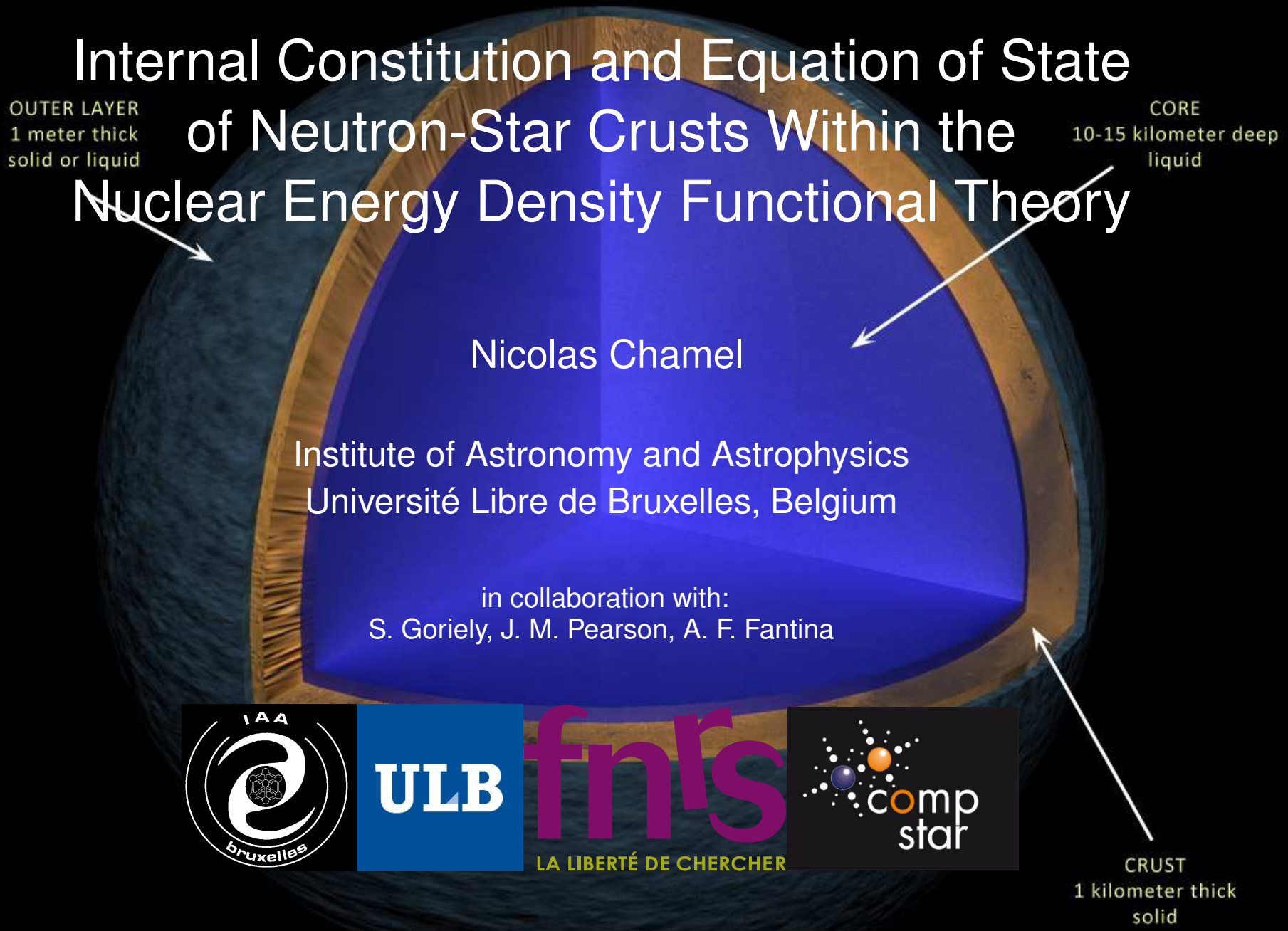

Nicolas Chamel

Institute of Astronomy and Astrophysics
Université Libre de Bruxelles, Belgium

in collaboration with:
S. Goriely, J. M. Pearson, A. F. Fantina

LA LIBERTÉ DE CHERCHER

XIIth Quark Conf. & the Hadron Spectrum, Thessaloniki, 28 August-4 September 2016

Punchline

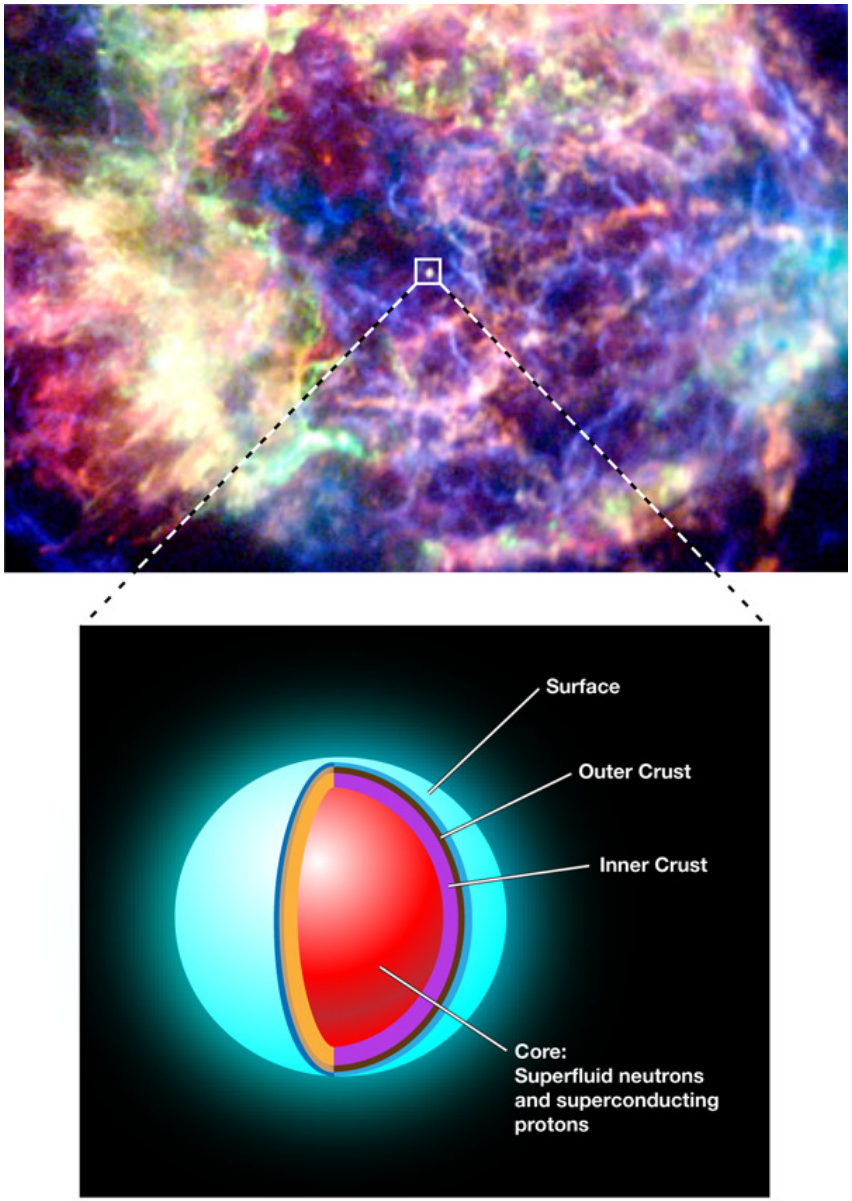

Neutron stars are not only made of neutrons !

Although the crust of a neutron star represents about $\sim 1\%$ of the mass and $\sim 10\%$ of the radius, it is related to various observations:

- pulsar sudden spin-ups,
- X-ray (super)bursts,
- thermal relaxation in transiently accreting stars,
- quasiperiodic oscillations in soft gamma-ray repeaters.

The crust of a neutron star: from atomic nuclei to nuclear pastas

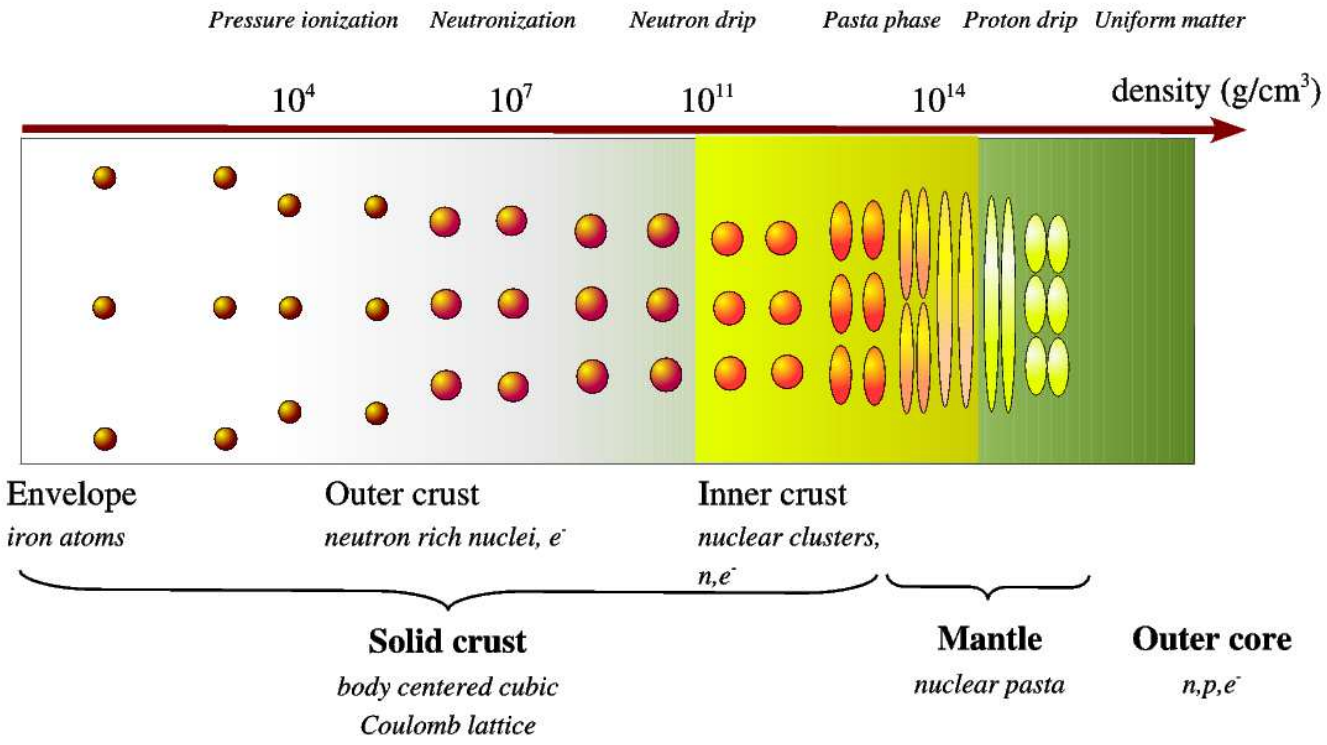

Chamel&Haensel, Living Reviews in Relativity 11 (2008), 10
http://relativity.livingreviews.org/Articles/lrr-2008-10/

The nuclear energy density functional theory provides a consistent and numerically tractable treatment of these different phases.

Nuclear energy density functional theory in a nut shell

The ground-state energy is obtained by minimizing a *functional* $E[n_q(\boldsymbol{r},\sigma;\boldsymbol{r'},\sigma'),\tilde{n}_q(\boldsymbol{r},\sigma;\boldsymbol{r'},\sigma')]$ of the **"normal" and "abnormal" density matrices** ($q = n, p$ for neutrons, protons)

$$n_q(\boldsymbol{r},\sigma;\boldsymbol{r'},\sigma') =< \Psi|c_q(\boldsymbol{r'}\sigma')^\dagger c_q(\boldsymbol{r}\sigma)|\Psi >,$$
$$\tilde{n}_q(\boldsymbol{r},\sigma;\boldsymbol{r'},\sigma') = -\sigma' < \Psi|c_q(\boldsymbol{r'}-\sigma')c_q(\boldsymbol{r}\sigma)|\Psi >,$$

where $c_q(\boldsymbol{r}\sigma)^\dagger$ and $c_q(\boldsymbol{r}\sigma)$ are the creation and destruction operators for nucleon at position $\boldsymbol{r}$ with spin $\sigma = \pm 1$.

In turn, the density matrices are expressed in terms of **independent quasiparticle states** $\varphi_{1k}^{(q)}(\boldsymbol{r})$ and $\varphi_{2k}^{(q)}(\boldsymbol{r})$ as

$$n_q(\boldsymbol{r},\sigma;\boldsymbol{r'},\sigma') = \sum_{k(q)} \varphi_{2k}^{(q)}(\boldsymbol{r},\sigma)\varphi_{2k}^{(q)}(\boldsymbol{r'},\sigma')^*$$
$$\tilde{n}_q(\boldsymbol{r},\sigma;\boldsymbol{r'},\sigma') = -\sum_{k(q)} \varphi_{2k}^{(q)}(\boldsymbol{r},\sigma)\varphi_{1k}^{(q)}(\boldsymbol{r'},\sigma')^* = -\sum_{k} \varphi_{1k}^{(q)}(\boldsymbol{r},\sigma)\varphi_{2k}^{(q)}(\boldsymbol{r'},\sigma')^*.$$

Duguet, Lecture Notes in Physics 879 (Springer-Verlag, 2014), p. 293

Dobaczewski & Nazarewicz, in "50 years of Nuclear BCS" (World Scientific Publishing, 2013), pp.40-60

Nuclear energy density functional theory in a nut shell

Constrained variations of the nuclear energy functional yield the self-consistent Hartree-Fock Bogoliubov (HFB) equations

$$\sum_{\sigma'} \int d^3r' \begin{pmatrix} h_q(\boldsymbol{r},\sigma;\boldsymbol{r'},\sigma') & \tilde{h}_q(\boldsymbol{r},\sigma;\boldsymbol{r'},\sigma') \\ \tilde{h}_q(\boldsymbol{r},\sigma;\boldsymbol{r'},\sigma') & -h_q(\boldsymbol{r},\sigma;\boldsymbol{r'},\sigma') \end{pmatrix} \begin{pmatrix} \psi_{1k}^{(q)}(\boldsymbol{r'},\sigma') \\ \psi_{2k}^{(q)}(\boldsymbol{r'},\sigma') \end{pmatrix}$$
$$= \begin{pmatrix} E_k^{(q)} + \mu_q & 0 \\ 0 & E_k^{(q)} - \mu_q \end{pmatrix} \begin{pmatrix} \psi_{1k}^{(q)}(\boldsymbol{r},\sigma) \\ \psi_{2k}^{(q)}(\boldsymbol{r},\sigma) \end{pmatrix},$$

where μ_q are the chemical potentials, and the non-local fields are defined by

$$h_q(\boldsymbol{r},\sigma;\boldsymbol{r'},\sigma') = \frac{\delta E}{\delta n_q(\boldsymbol{r},\sigma;\boldsymbol{r'},\sigma')}, \qquad \tilde{h}_q(\boldsymbol{r},\sigma;\boldsymbol{r'},\sigma') = \frac{\delta E}{\delta \tilde{n}_q(\boldsymbol{r},\sigma;\boldsymbol{r'},\sigma')}.$$

Problem: we do not know what the exact functional is... We have thus to rely on phenomenological functionals.

Phenomenological nuclear energy density functionals

For simplicity, the functional is generally written as

$$E = \int \mathcal{E}\Big[n_q(\boldsymbol{r}), \nabla n_q(\boldsymbol{r}), \tau_q(\boldsymbol{r}), \boldsymbol{J}_q(\boldsymbol{r}), \tilde{n}_q(\boldsymbol{r})\Big]\, \mathrm{d}^3\boldsymbol{r}$$

where ($\boldsymbol{\sigma}_{\sigma\sigma'}$ denotes the Pauli spin matrices)

$$n_q(\boldsymbol{r}) = \sum_{\sigma=\pm 1} n_q(\boldsymbol{r}, \sigma; \boldsymbol{r}, \sigma), \quad \tilde{n}_q(\boldsymbol{r}) = \sum_{\sigma=\pm 1} \tilde{n}_q(\boldsymbol{r}, \sigma; \boldsymbol{r}, \sigma)$$

$$\tau_q(\boldsymbol{r}) = \sum_{\sigma=\pm 1} \int \mathrm{d}^3\boldsymbol{r}'\, \delta(\boldsymbol{r} - \boldsymbol{r}') \nabla \cdot \nabla' n_q(\boldsymbol{r}, \sigma; \boldsymbol{r}', \sigma)$$

$$\boldsymbol{J}_q(\boldsymbol{r}) = -\mathrm{i} \sum_{\sigma,\sigma'=\pm 1} \int \mathrm{d}^3\boldsymbol{r}'\, \delta(\boldsymbol{r} - \boldsymbol{r}') \nabla n_q(\boldsymbol{r}, \sigma; \boldsymbol{r}', \sigma') \times \boldsymbol{\sigma}_{\sigma'\sigma}$$

Such semi-local functionals can be constructed from Skyrme type **zero-range effective nucleon-nucleon interactions** thus avoiding self-interaction errors.

Chamel, Phys. Rev. C 82, 061307(R) (2010).

Brussels-Montreal Skyrme functionals (BSk)

These functionals were fitted to both experimental data and N-body calculations using realistic forces.

Experimental data:

- all atomic masses with $Z, N \geq 8$ from the Atomic Mass Evaluation (root-mean square deviation: 0.5-0.6 MeV)
- nuclear charge radii
- incompressibility $K_v = 240 \pm 10$ MeV (ISGMR)
  Colò et al., Phys.Rev.C70, 024307 (2004).

N-body calculations using realistic forces:

- equation of state of pure neutron matter
- $^1S_0$ pairing gaps in nuclear matter
- effective masses in nuclear matter
- stability against spin and spin-isospin fluctuations

Chamel et al., Acta Phys. Pol. B46, 349(2015)

Phenomenological corrections for atomic nuclei

For atomic nuclei, we add the following corrections to the HFB energy:

- Wigner energy

$$E_W = V_W \exp\left\{ -\lambda \left(\frac{N-Z}{A} \right)^2 \right\} + V'_W |N-Z| \exp\left\{ -\left(\frac{A}{A_0} \right)^2 \right\}$$

$V_W \sim -2$ MeV, $V'_W \sim 1$ MeV, $\lambda \sim 300$ MeV, $A_0 \sim 20$

- rotational and vibrational spurious collective energy

$$E_{\rm coll} = E_{\rm rot}^{\rm crank} \Big\{ b \ \tanh(c|\beta_2|) + d|\beta_2| \ \exp\{-I(|\beta_2| - \beta_2^0)^2\} \Big\}$$

This latter correction was shown to be in good agreement with calculations using 5D collective Hamiltonian.
Goriely, Chamel, Pearson, Phys.Rev.C82,035804(2010).

In this way, these collective effects do not contaminate the parameters (≤ 20) of the functional.

Brussels-Montreal Skyrme functionals

Main features of the latest functionals:

- **fit to realistic $^1S_0$ pairing gaps (no self-energy)** (BSk16-17)
  Chamel, Goriely, Pearson, Nucl.Phys.A812,72 (2008)
  Goriely, Chamel, Pearson, PRL102,152503 (2009).
- **removal of spurious spin-isospin instabilities** (BSk18)
  Chamel, Goriely, Pearson, Phys.Rev.C80,065804(2009)
- **fit to realistic neutron-matter equations of state** (BSk19-21)
  Goriely, Chamel, Pearson, Phys.Rev.C82,035804(2010)
- **fit to different symmetry energies** (BSk22-26)
  Goriely, Chamel, Pearson, Phys.Rev.C88,024308(2013)
- **optimal fit of the 2012 AME** - rms 0.512 MeV (BSk27*)
  Goriely, Chamel, Pearson, Phys.Rev.C88,061302(R)(2013)
- **generalized spin-orbit coupling** (BSk28-29)
  Goriely, Nucl.Phys.A933,68(2015).
- **fit to realistic $^1S_0$ pairing gaps with self-energy** (BSk30-32)
  Goriely, Chamel, Pearson, Phys.Rev. C93,034337(2016).

Neutron-matter equation of state

The neutron-matter equation of state obtained with our functionals are consistent with microscopic calculations using realistic interactions:

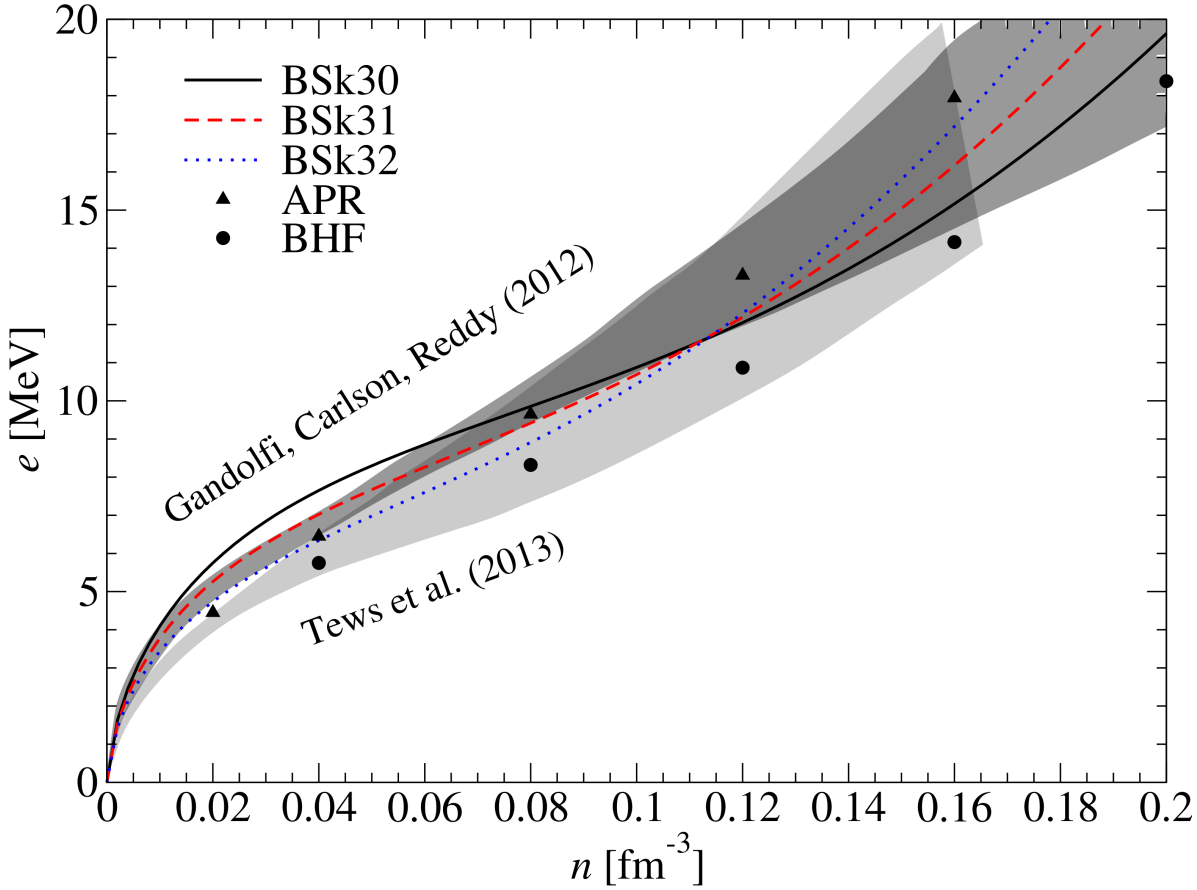

$^1S_0$ pairing gaps in nuclear matter

For consistency, we considered the gaps obtained from extended BHF calculations since effective masses as well as equations of state have been also calculated with this approach.

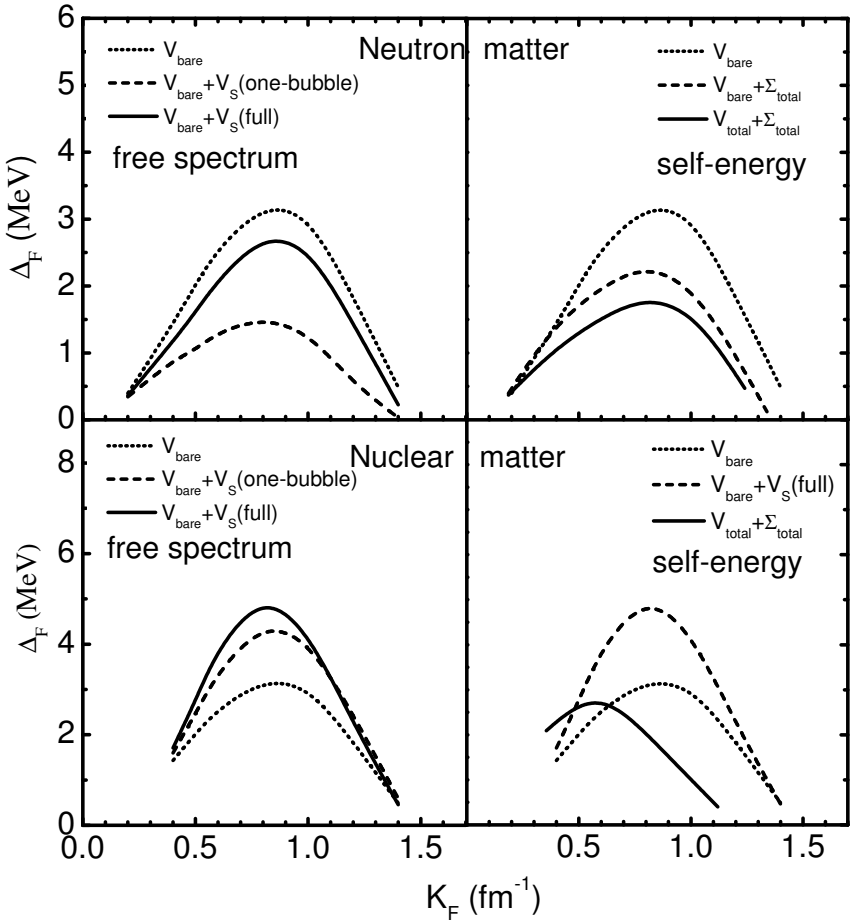

For comparison, we fitted functionals to different approximations for the gaps:

- **BCS**: BSk16
- **polarization+free spectrum**: BSk17-BSk29
- **polarization+self-energy**: BSk30-32.

Cao et al., Phys.Rev.C74,064301(2006)

Nucleon effective masses

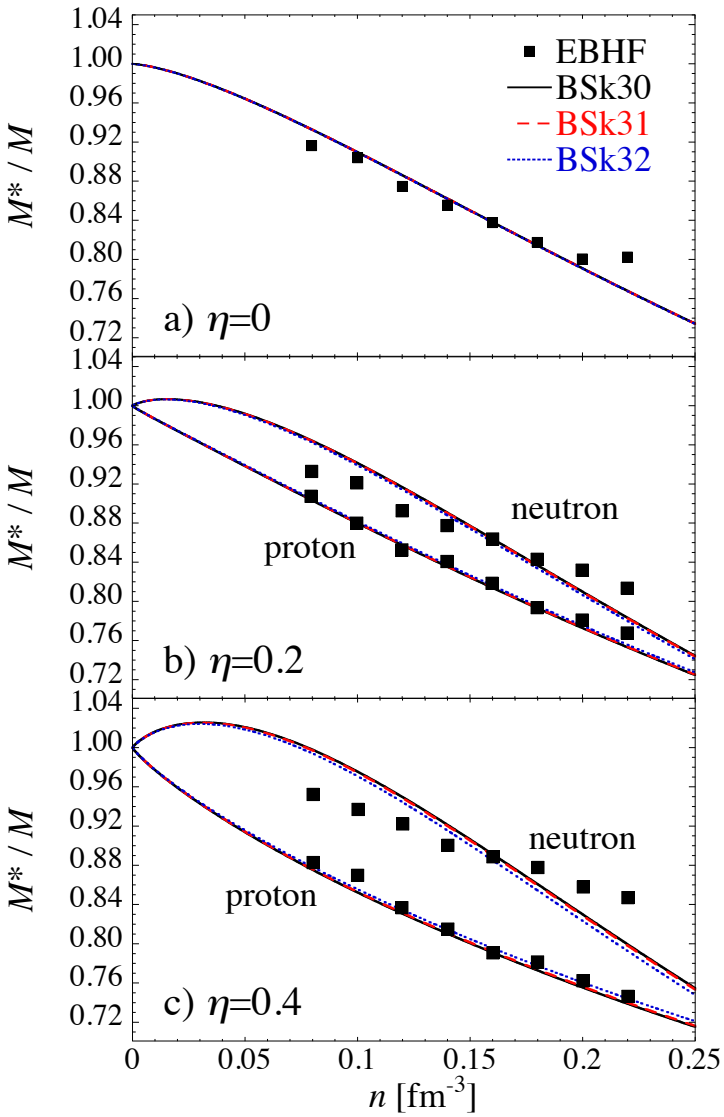

Effective masses obtained with our functionals are consistent with giant resonances in finite nuclei and many-body calculations in infinite nuclear matter.

This was achieved using **generalized Skyrme interactions** with density dependent t_1 and t_2 terms, initially introduced to remove spurious instabilities. *Chamel, Goriely, Pearson, Phys.Rev.C80,065804(2009)*

EBHF calculations from *Cao et al.,Phys.Rev.C73,014313(2006)*.

Description of the outer crust of a neutron star

Main assumptions:

- atoms are fully pressure ionized $\rho \gg 10AZ$ g cm^{-3}
- the crust consists of a perfect body-centered cubic crystal

  $$T < T_m \approx 1.3 \times 10^5 Z^2 \left(\frac{\rho_6}{A}\right)^{1/3} \mathrm{K} \qquad \rho_6 \equiv \rho/10^6 \ \mathrm{g\ cm^{-3}}$$
- electrons are uniformly distributed and are highly degenerate
- matter is fully "catalyzed"

The only microscopic inputs are nuclear masses. We have made use of the experimental data from the Atomic Mass Evaluation complemented with our HFB mass tables available at
`http://www.astro.ulb.ac.be/bruslib/`
Pearson,Goriely,Chamel,Phys.Rev.C83,065810(2011)

Electron exchange and polarization effects are included using the expressions given by *Chamel & Fantina,Phys.Rev.D93, 063001 (2016)*

Composition of the outer crust of a neutron star

The composition of the crust is completely determined by experimental nuclear masses down to about 200m for a $1.4 M_{\odot}$ neutron star with a 10 km radius

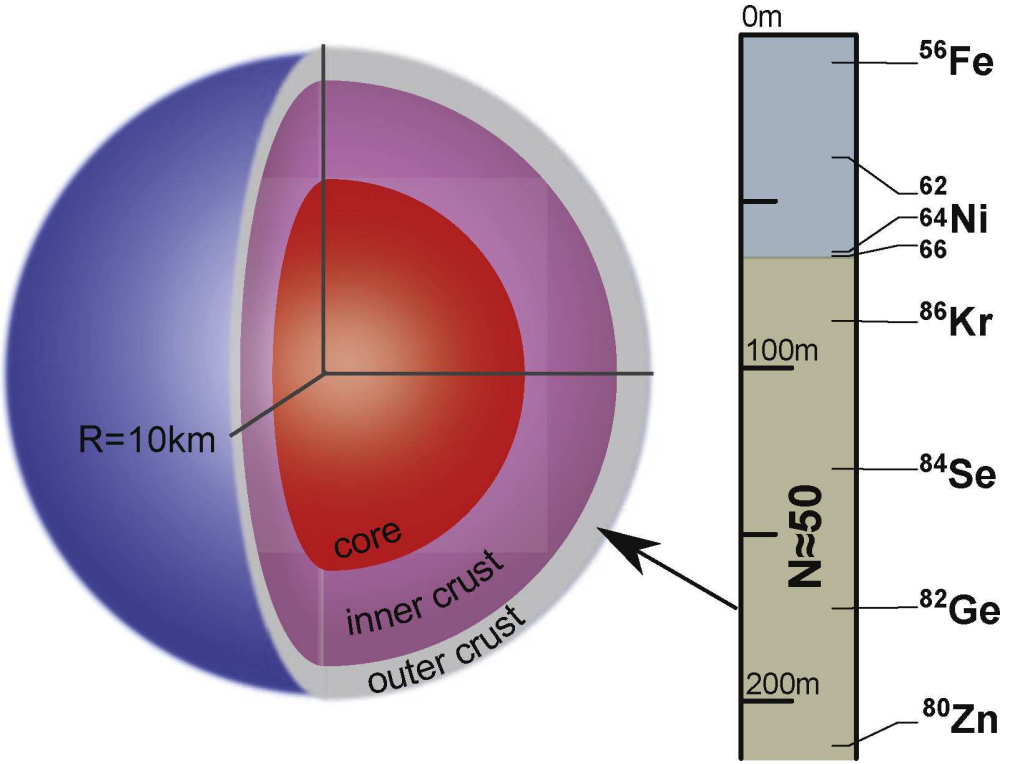

Pearson,Goriely,Chamel,Phys.Rev.C83,065810(2011)
Kreim, Hempel, Lunney, Schaffner-Bielich, Int.J.M.Spec.349-350,63(2013)
Wolf et al.,PRL 110,041101(2013)

Composition of the outer crust of a neutron star

Role of the symmetry energy

HFB-22-25 were fitted to different values of the symmetry energy coefficient at saturation, from $J = 29$ MeV (HFB-25) to $J = 32$ MeV (HFB-22).

HFB-22 (32)	HFB-24 (30)	HFB-25 (29)
^{79}Cu	-	-
^{82}Zn	-	-
^{78}Ni	^{78}Ni	^{78}Ni
^{80}Ni	^{80}Ni	-
-	-	^{126}Ru
^{124}Mo	^{124}Mo	^{124}Mo
^{122}Zr	^{122}Zr	^{122}Zr
^{121}Y	^{121}Y	^{121}Y
-	^{120}Sr	^{120}Sr
^{122}Sr	^{122}Sr	^{122}Sr
^{124}Sr	^{124}Sr	-
^{128}Sr	-	-

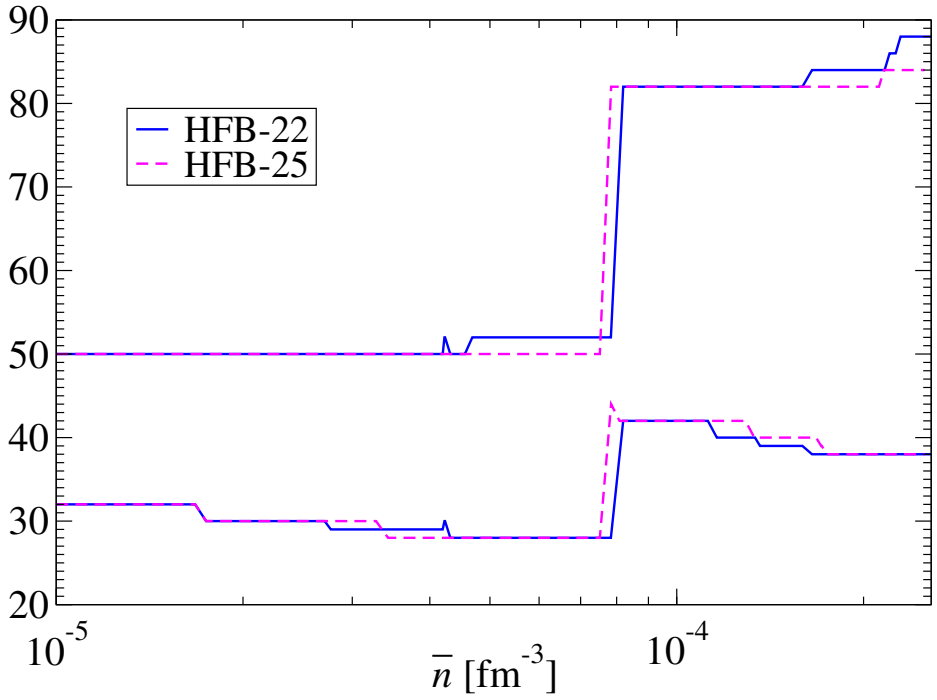

Composition of the outer crust of a neutron star

Role of the symmetry energy

HFB-22-25 were fitted to different values of the symmetry energy coefficient at saturation, from $J = 29$ MeV (HFB-25) to $J = 32$ MeV (HFB-22).

HFB-22 (32)	HFB-24 (30)	HFB-25 (29)
^{79}Cu	-	-
^{82}Zn	-	-
^{78}Ni	^{78}Ni	^{78}Ni
^{80}Ni	^{80}Ni	-
-	-	^{126}Ru
^{124}Mo	^{124}Mo	^{124}Mo
^{122}Zr	^{122}Zr	^{122}Zr
^{121}Y	^{121}Y	^{121}Y
-	^{120}Sr	^{120}Sr
^{122}Sr	^{122}Sr	^{122}Sr
^{124}Sr	^{124}Sr	-
^{128}Sr	-	-

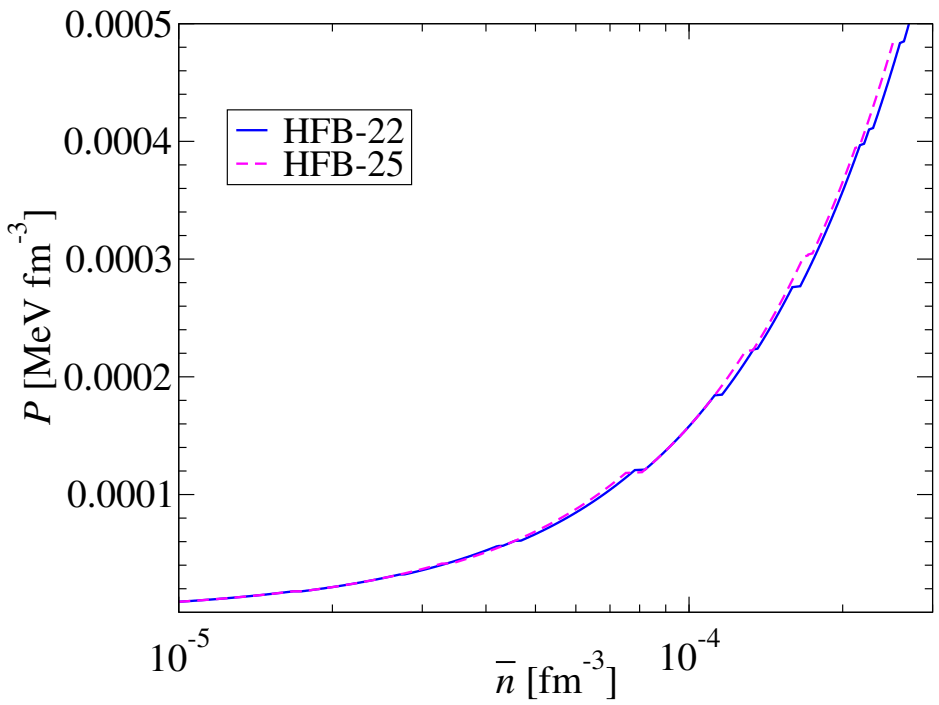

Composition of the outer crust of a neutron star

Role of the spin-orbit coupling

HFB-24: $v_{ij}^{\rm so} = \frac{\rm i}{\hbar^2} W_0(\boldsymbol{\sigma}_i + \boldsymbol{\sigma}_j) \cdot \boldsymbol{p}_{ij} \times \delta(\boldsymbol{r}_{ij}) \boldsymbol{p}_{ij}$

HFB-28: $v_{ij}^{\rm so} \to v_{ij}^{\rm so} + \frac{\rm i}{\hbar^2} W_1(\boldsymbol{\sigma}_i + \boldsymbol{\sigma}_j) \cdot \boldsymbol{p}_{ij} \times (n_{qi} + n_{qj})^{\nu} \delta(\boldsymbol{r}_{ij}) \boldsymbol{p}_{ij}$

HFB-29: $\mathcal{E}_{\rm so} = \frac{1}{2}\left[\boldsymbol{J} \cdot \nabla n + (1 + y_w) \sum_q \boldsymbol{J_q} \cdot \nabla n_q\right]$

HFB-28	HFB-29	HFB-24
^{79}Cu	^{79}Cu	-
^{78}Ni	^{78}Ni	^{78}Ni
^{128}Pd	-	-
^{80}Ni	-	^{80}Ni
^{126}Ru	^{126}Ru	-
^{124}Mo	^{124}Mo	^{124}Mo
^{122}Zr	^{122}Zr	^{122}Zr
-	^{121}Y	^{121}Y
^{120}Sr	^{120}Sr	^{120}Sr
^{122}Sr	^{122}Sr	^{122}Sr
^{124}Sr	^{124}Sr	^{124}Sr

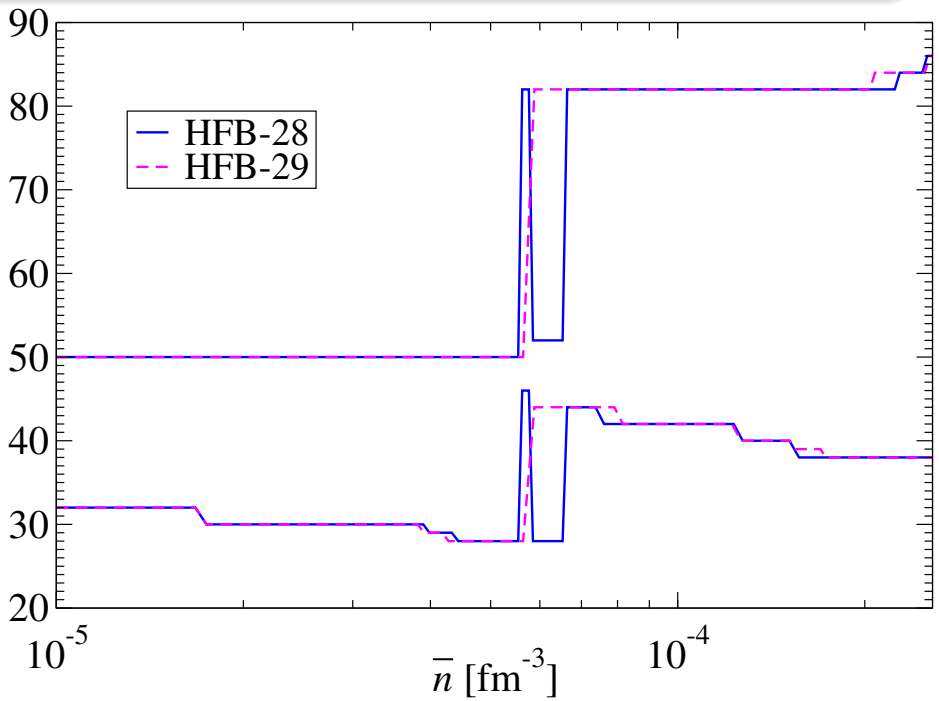

Composition of the outer crust of a neutron star

Role of the spin-orbit coupling

HFB-24: $v_{ij}^{\rm so} = \frac{\rm i}{\hbar^2} W_0(\boldsymbol{\sigma}_i + \boldsymbol{\sigma}_j) \cdot \boldsymbol{p}_{ij} \times \delta(\boldsymbol{r}_{ij}) \boldsymbol{p}_{ij}$

HFB-28: $v_{ij}^{\rm so} \to v_{ij}^{\rm so} + \frac{\rm i}{\hbar^2} W_1(\boldsymbol{\sigma}_i + \boldsymbol{\sigma}_j) \cdot \boldsymbol{p}_{ij} \times (n_{qi} + n_{qj})^{\nu} \delta(\boldsymbol{r}_{ij}) \boldsymbol{p}_{ij}$

HFB-29: $\mathcal{E}_{\rm so} = \frac{1}{2}\left[\boldsymbol{J} \cdot \nabla n + (1 + y_w) \sum_q \boldsymbol{J_q} \cdot \nabla n_q\right]$

HFB-28	HFB-29	HFB-24
^{79}Cu	^{79}Cu	-
^{78}Ni	^{78}Ni	^{78}Ni
^{128}Pd	-	-
^{80}Ni	-	^{80}Ni
^{126}Ru	^{126}Ru	-
^{124}Mo	^{124}Mo	^{124}Mo
^{122}Zr	^{122}Zr	^{122}Zr
-	^{121}Y	^{121}Y
^{120}Sr	^{120}Sr	^{120}Sr
^{122}Sr	^{122}Sr	^{122}Sr
^{124}Sr	^{124}Sr	^{124}Sr

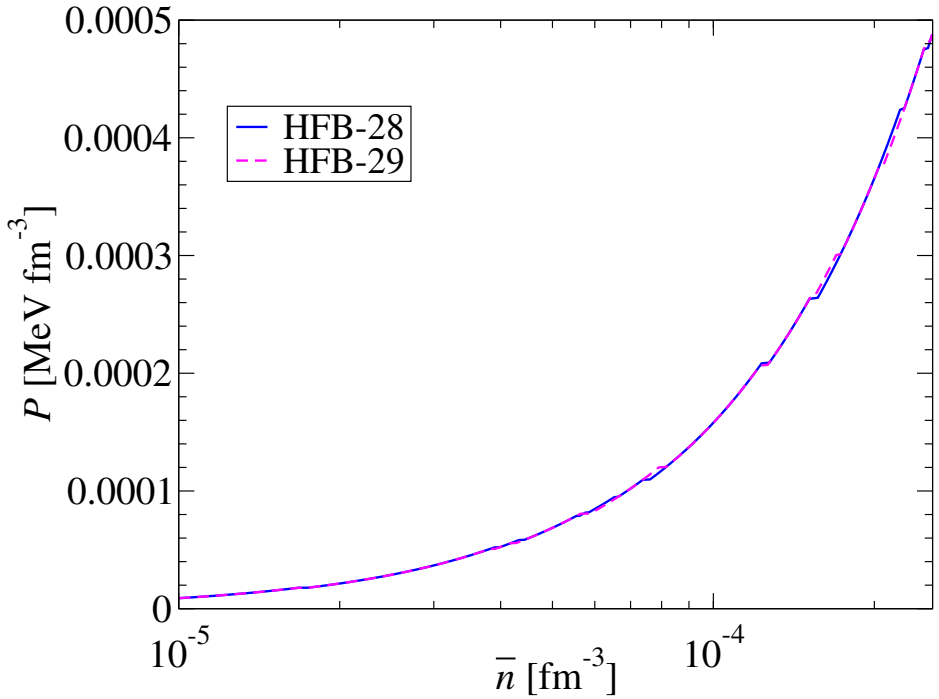

Composition of the outer crust of a neutron star

Role of nuclear pairing

HFB-27* is based on an empirical pairing functional.
HFB-29 (HFB-30) was fitted to extended Brueckner Hartree-Fock $^1S_0$ pairing gaps in symmetric and neutron matter including medium polarization effects without (with) self-energy effects.

HFB-27*	HFB-29	HFB-30
-	^{79}Cu	-
^{78}Ni	^{78}Ni	^{78}Ni
-	-	^{80}Ni
^{126}Ru	^{126}Ru	^{126}Ru
^{124}Mo	^{124}Mo	^{124}Mo
^{122}Zr	^{122}Zr	^{122}Zr
-	^{121}Y	^{121}Y
^{120}Sr	^{120}Sr	^{120}Sr
^{122}Sr	^{122}Sr	^{122}Sr
^{124}Sr	^{124}Sr	^{124}Sr

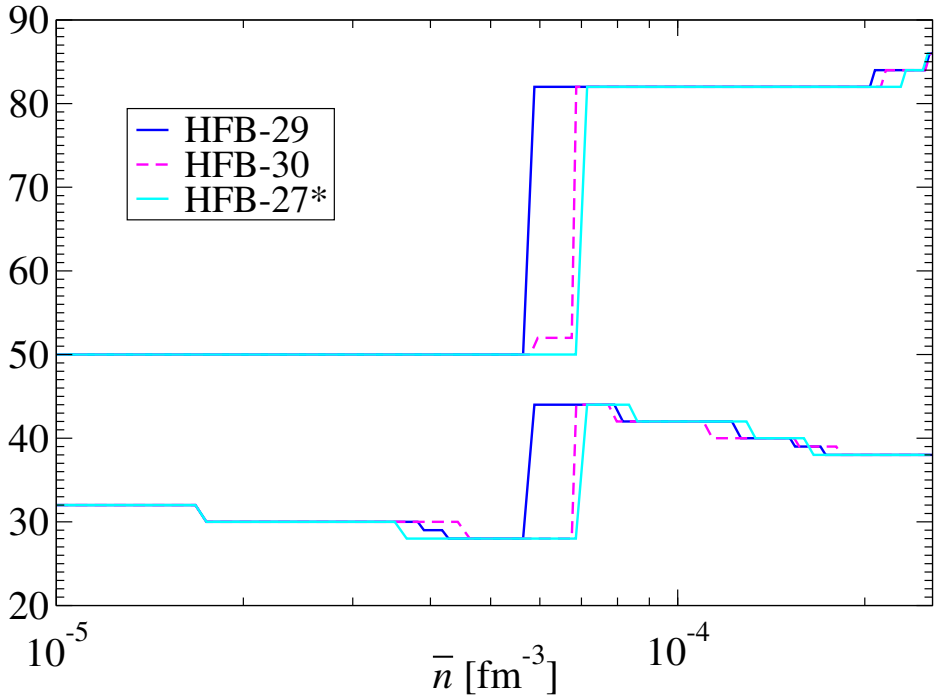

Composition of the outer crust of a neutron star

Role of nuclear pairing

HFB-27* is based on an empirical pairing functional.
HFB-29 (HFB-30) was fitted to extended Brueckner Hartree-Fock $^1S_0$ pairing gaps in symmetric and neutron matter including medium polarization effects without (with) self-energy effects.

HFB-27*	HFB-29	HFB-30
-	^{79}Cu	-
^{78}Ni	^{78}Ni	^{78}Ni
-	-	^{80}Ni
^{126}Ru	^{126}Ru	^{126}Ru
^{124}Mo	^{124}Mo	^{124}Mo
^{122}Zr	^{122}Zr	^{122}Zr
-	^{121}Y	^{121}Y
^{120}Sr	^{120}Sr	^{120}Sr
^{122}Sr	^{122}Sr	^{122}Sr
^{124}Sr	^{124}Sr	^{124}Sr

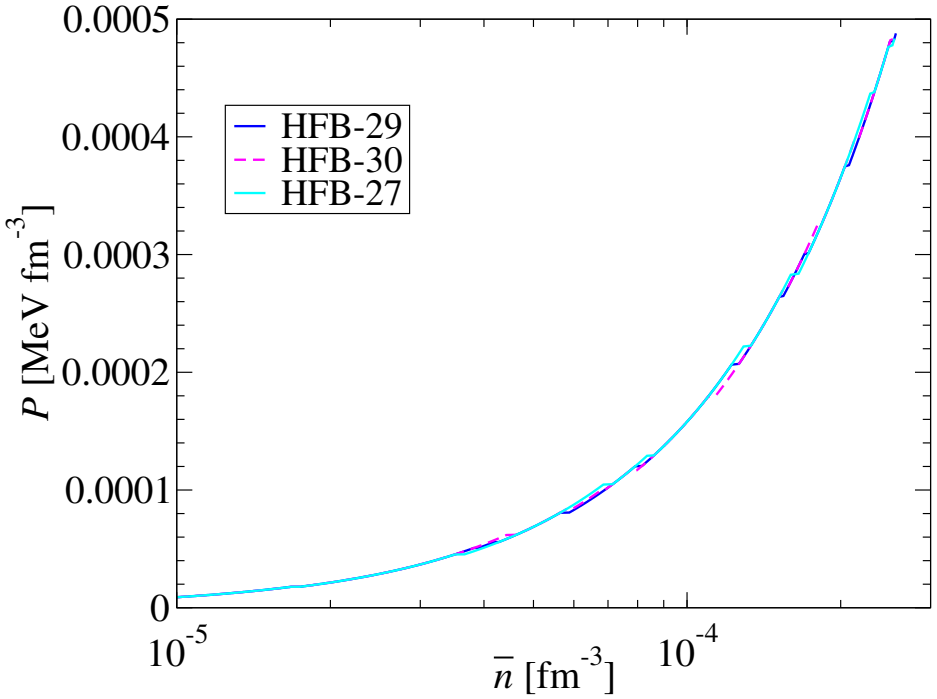

Neutron-drip transition: general considerations

With increasing pressure, nuclei become progressively more neutron rich until neutrons start to drip out.

At this point, nuclei are actually stable against neutron emission but are unstable against *electron captures* accompanied by neutron emission

$$ {}^{A}_{Z}\mathrm{X} + \Delta Z e^- \rightarrow {}^{A-\Delta N}_{Z-\Delta Z}\mathrm{Y} + \Delta N\, n + \Delta Z\, \nu_e $$

According to the cold catalyzed matter hypothesis, all kinds of reactions are allowed: the ground state is reached for $\Delta Z = Z$ and $\Delta N = A$ (different conditions prevail in accreted crusts).

	outer crust	drip line	$\rho_{\rm drip}$ (g cm^{-3})	$P_{\rm drip}$ (dyn cm^{-2})
HFB-19	^{126}Sr (0.73)	^{121}Sr (-0.62)	4.40×10^{11}	7.91×10^{29}
HFB-20	^{126}Sr (0.48)	^{121}Sr (-0.71)	4.39×10^{11}	7.89×10^{29}
HFB-21	^{124}Sr (0.83)	^{121}Sr (-0.33)	4.30×10^{11}	7.84×10^{29}

$\rho_{\rm drip}$ and $P_{\rm drip}$ can be expressed by simple analytical formulas.
Chamel, Fantina, Zdunik, Haensel, Phys. Rev. C91,055803(2015).

Description of neutron star crust beyond neutron drip

4th order Extended Thomas-Fermi+Strutinsky Integral (ETFSI):

- $\tau_q(\boldsymbol{r})$ and $\boldsymbol{J_q}(\boldsymbol{r})$ are expanded into $n_q(\boldsymbol{r})$ and its gradients
- minimization of the energy yields $\lambda_q = \dfrac{\delta E}{\delta n_q(r)}$ whose solutions are $\widetilde{n_q}(\boldsymbol{r})$ and $E[\widetilde{n_q}(\boldsymbol{r})] = E_{\mathrm{ETF}}$
- proton shell effects are added perturbatively using the Strutinsky integral theorem $E \approx E_{\mathrm{ETF}} + \delta E_p$ (neutron shell effects are expected to be mucher smaller, $|\delta E_n| \ll |\delta E_p|$)

$$\delta E_p = \sum_k v_k^2 \varepsilon_k - \int d^3\boldsymbol{r} \left\{ \frac{\hbar^2}{2\widetilde{M_p}^\star(\boldsymbol{r})} \widetilde{\tau_p}(\boldsymbol{r}) + \widetilde{n_p}(\boldsymbol{r}) \widetilde{U_p}(\boldsymbol{r}) + \widetilde{\boldsymbol{J_p}}(\boldsymbol{r}) \cdot \widetilde{\boldsymbol{W_p}}(\boldsymbol{r}) \right\} - \sum_k \frac{\Delta_k^2}{4E_k}$$

where $\left\{ -\boldsymbol{\nabla} \cdot \dfrac{\hbar^2}{2\widetilde{M_p}^\star(\boldsymbol{r})} \boldsymbol{\nabla} + \widetilde{U_p}(\boldsymbol{r}) - \mathrm{i}\widetilde{\boldsymbol{W_p}}(\boldsymbol{r}) \cdot \boldsymbol{\nabla} \times \boldsymbol{\sigma} \right\} \varphi_k(\boldsymbol{r}) = \varepsilon_k \varphi_k(\boldsymbol{r})$

$$E_k = \sqrt{(\varepsilon_k - \lambda_p)^2 + \Delta_k^2}, \qquad v_k^2 = \frac{1}{2}\left(1 - \frac{\varepsilon_k - \lambda_p}{E_k}\right)$$

$$\Delta_k = -\frac{1}{4} \sum_l \bar{v}^{\mathrm{pair}}_{k\bar{k},l\bar{l}} \frac{\Delta_l}{E_l}$$

Description of neutron star crust beyond neutron drip

In order to further speed-up the calculations, we make the following approximations:

- neutron-proton clusters are spherical and $n_q(\boldsymbol{r})$ are parametrized as $n_q(r) = n_{Bq} + n_{\Lambda q} f_q(r)$, where
$$f_q(r) = \frac{1}{1 + \exp\left\{\left(\frac{C_q - R}{r - R}\right)^2 - 1\right\} \exp\left(\frac{r - C_q}{a_q}\right)}$$
- the lattice energy is computed using the Wigner-Seitz method,
- electrons are uniformly distributed.

Pearson,Chamel,Pastore,Goriely,Phys.Rev.C91, 018801 (2015).
Pearson,Chamel,Goriely,Ducoin,Phys.Rev.C85,065803(2012).

Advantages of the ETFSI method:

- very fast approximation to the full HF+BCS equations
- avoids the difficulties related to boundary conditions
  Chamel et al.,Phys.Rev.C75(2007),055806.

Structure of nonaccreting neutron star crusts

With increasing density, the clusters keep essentially the same size but become more and more dilute.

The crust-core transition predicted by the ETFSI method agrees very well with the instability analysis of homogeneous nuclear matter.

	$\bar{n}_{cc}$ (fm^{-3})	P_{cc} (MeV fm^{-3})
BSk27*	0.0919	0.439
BSk21	0.0809	0.268
BSk20	0.0854	0.365
BSk19	0.0885	0.428

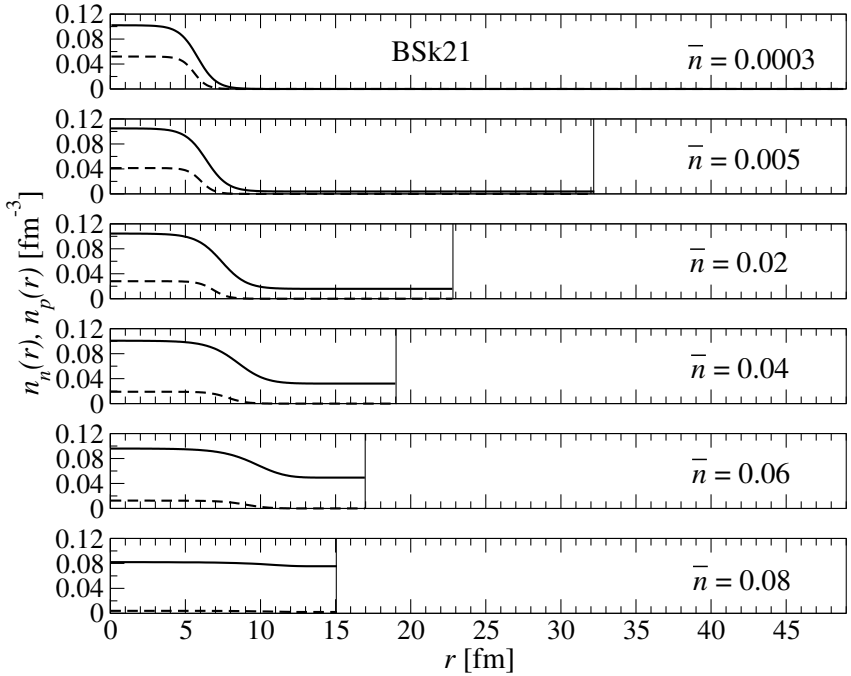

Chamel et al., Acta Phys. Pol.46,349(2015).
Pearson,Chamel,Goriely,Ducoin,Phys.Rev.C85,065803(2012).

The crust-core transition is very smooth.

Role of proton shell effects on the composition of the inner crust of a neutron star

- The ordinary nuclear shell structure seems to be preserved apart from $Z = 40$ (quenched spin-orbit?).
- The energy differences between different configurations become very small as the density increases!

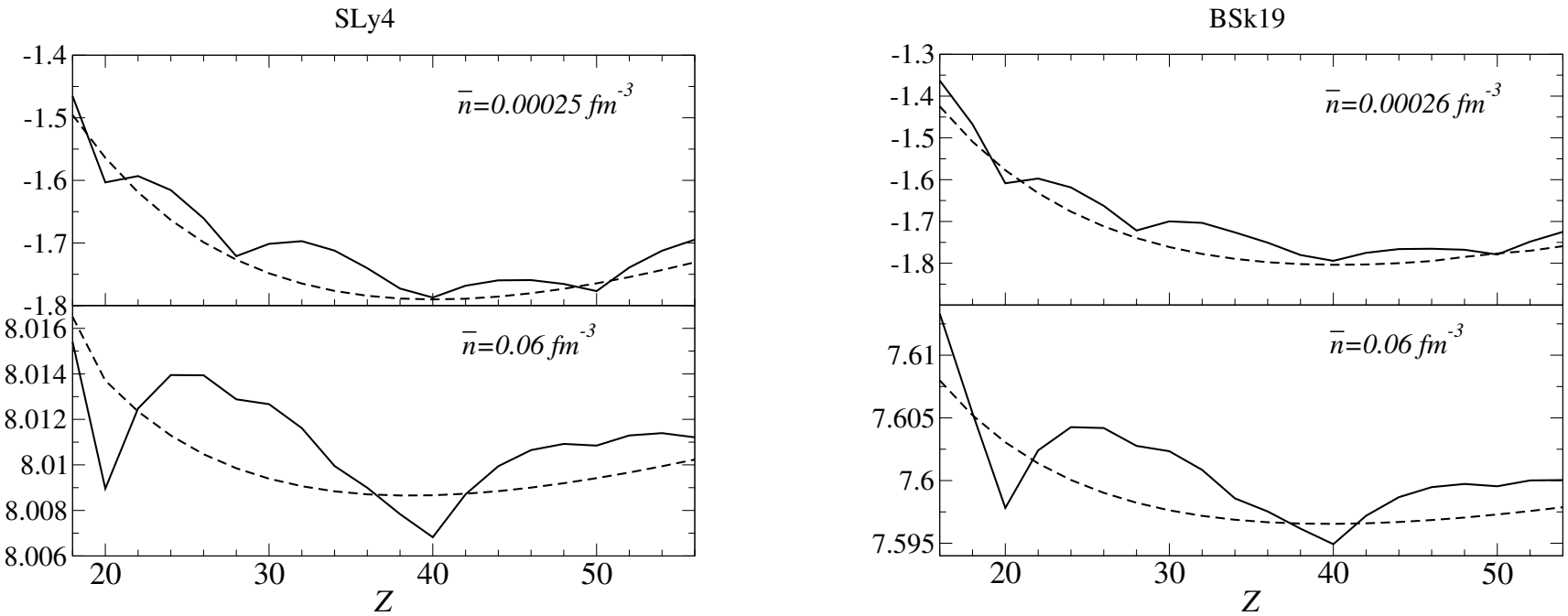

ETF: dashed lines - ETFSI: solid lines

Role of proton pairing on the composition of the inner crust of a neutron star

Proton shell effects are washed out due to pairing.

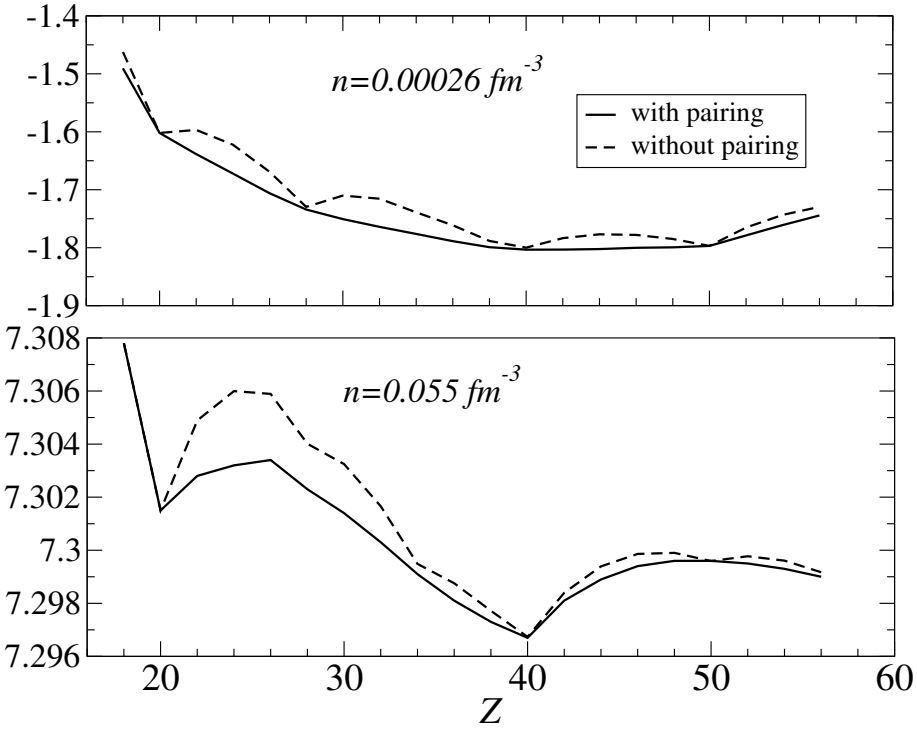

Example with BSk21.

At low densities, $Z = 42$ is energetically favored over $Z = 40$, but by less than 5×10^{-4} MeV per nucleon.

A large range of values of Z could thus be present in a real neutron-star crust.

Pearson,Chamel,Pastore,Goriely,Phys.Rev.C91, 018801 (2015).

Due to proton pairing, the inner crust of a neutron star is expected to contain many impurities.

Conclusions

- We have employed accurately calibrated nuclear energy density functionals to describe consistently both the outer and inner crusts of a neutron star.
- These functionals were fitted to essentially all experimental nuclear masses and was also constrained to reproduce realistic nuclear-matter calculations.
- Whereas the equation of state of the outer crust is fairly well known, its composition is found to be sensitive to the details of the nuclear structure (e.g. spin-orbit coupling, pairing).
- The constitution of the inner crust is much more uncertain due to the tiny energy differences between different configurations (nuclear pastas?).
- Systematic studies of the inner crust are under way.